Electrochimica Acta 159 (2015) 210–218

Contents lists available at ScienceDirect

Electrochimica Acta

journal homepage: www.elsevier.com/locate/electacta

Kinetics of the hydrogen evolution on nickel in alkaline solution: new insight from rotating disk electrode and impedance spectroscopy analysis

Esteban A. Franceschini [a,*], Gabriela I. Lacconi [b], Horacio R. Corti [a,c]

[a] Departamento de Física de la Materia Condensada, Centro Atómico Constituyentes, Comisión Nacional de Energía Atómica, Av. Gral. Paz 1499 (B1650KNA) San Martín, Buenos Aires, Argentina
[b] INFIQC-CONICET, Dto. de Fisicoquímica – Facultad de Ciencias Químicas, Universidad Nacional de Córdoba, Ciudad Universitaria, 5000, Córdoba, Argentina
[c] Departamento de Química Inorgánica, Analítica y Química Física and INQUIMAE-CONICET, Facultad de Ciencias Exactas y Naturales, Universidad de Buenos Aires, Ciudad Universitaria, Pabellón II, C1428EHA, Buenos Aires, Argentina

ARTICLE INFO

Article history:
Received 12 November 2014
Received in revised form 2 January 2015
Accepted 22 January 2015
Available online 24 January 2015

Keywords:
Hydrogen Evolution
Nickel
Rotating Disk Electrode
Electrochemical Impedance
Ageing

ABSTRACT

Nickel catalysts were characterized for the hydrogen evolution reaction (HER) using rotating disk electrode (RDE) and electrochemical impedance spectroscopy (EIS). The theoretical Levich slope was calculated on the basis of the HER mechanism in alkaline solution. Kinetic and thermodynamic parameters of the reaction were obtained for fresh polished nickel electrode (Ni_f), and for nickel after a quick chronoamperometric aging procedure (Ni_{pc}). Koutecky-Levich analysis indicated that the rate determining step on Ni_f is the one-electron Volmer reaction, while for Ni_{pc} decreases from one to 0.68 and exhibits a strong temperature dependence. A loss of catalytic activity, corresponding to an increase of 0.3 V of the HER onset potential, was observed after aging. Furthermore, from the EIS-Tafel analysis we concluded that the H adsorption changes from a Langmuir type for Ni_f, to a Temkin type for Ni_{pc}.

1. Introduction

The hydrogen evolution reaction (HER) is one of the most frequently studied electrochemical reactions for different reasons. First, the reaction takes place through a limited number of reaction steps with only one reaction intermediate involved [1–5]. Second, it has an industrial/technological interest in the alkaline water electrolysis [6–8], where nickel-based materials are used as a cathode.

There are a large number of works directed toward characterize the mechanism involved in the hydrogen evolution. The general mechanism of HER in alkaline solution on nickel electrodes, is based on the following three steps [2,9,10]:

$$Ni + H_2O + e^- \underset{k_{-V}}{\overset{k_V}{\rightleftharpoons}} Ni\cdots H_{ad} + HO^- \quad (Volmer\ Reaction)$$

$$2Ni\cdots H_{ad} \underset{k_{-T}}{\overset{k_T}{\rightleftharpoons}} 2Ni + H_2 \quad (Tafel Reaction)$$

$$Ni\cdots H_{ad} + H_2O + e^- \underset{k_{-H}}{\overset{k_H}{\rightleftharpoons}} Ni + HO^- + H_2 \quad (Heyrovsky Reaction)$$

In a simple thermodynamic analysis, entropy change for the Volmer reaction is negative, since the H adsorption orders the system, while Heyrovsky and Tafel reactions have positive entropy changes due to the desorption of one and two H_{ad}, respectively, to release $H_{2(g)}$. For the Heyrovsky reaction an additional decrease of entropy, as compared to the Tafel reaction, is promoted by the hydration of the HO^- ions [11].

There are several results reported for HER kinetics on nickel in alkaline solutions, where a Tafel slope close to $-0.120\,V\,dec^{-1}$ is commonly observed [11–15]. This indicates that, under these conditions, the Volmer reaction with the transference of one electron is the rate-determining step, making irrelevant the analysis of the Tafel and Heyrovsky steps [11,16].

RDE technique provides a large number of highly reproducible kinetics parameters, including those related to surface electrode passivation under controlled conditions. As far as we know, there are few RDE studies of the HER on nickel electrodes [17–19], and there is no information of Koutecky-Levich and Conway transfer coefficients in literature. Those parameters would allow establish the mechanistic and thermodynamic parameters affecting HER catalysis.

Ni cathodes exhibit a significant decrease of their HER activity after several hours of electrolysis [20–25]. Polished Ni surfaces exposed to air become coated with a bilayer composed of α-Ni

* Corresponding author. Fax: 5411 67717121.
E-mail address: efrances@tandar.cnea.gov.ar (E.A. Franceschini).

http://dx.doi.org/10.1016/j.electacta.2015.01.110
0013-4686/

$(OH)_2$ and NiO_x. At potentials lower than the reversible hydrogen electrode (RHE), the bilayer reduces to Ni metal, and forming α-NiH_x and β-NiH_x [22–24,26] contributing to the decrease of HER activity [22,24]. Small amounts of β-NiH_x was detected by galvanostatic pulses applied to nickel electrodes in alkaline solutions [24]. Hall et al. [27] found that Ni polished surfaces in this media are covered by a α-$Ni(OH)_2/NiO_x$ bilayer that incorporates H atoms deep into the electrode. In concentrated alkaline solutions and large cathodic current densities, α-NiH_x and β-NiH_x can be formed at the electrode surface, while NiO_x, α-Ni $(OH)_2$, β-$Ni(OH)_2$, and β-NiOOH can be reduced to Ni on subsequent cathodic polarization. However, repeated oxidation and reduction cycles introduce strains and mechanical failures are found on the electrode surface.

Although the mechanism of HER on nickel electrodes has been widely studied, the kinetics and electrochemical impedance spectroscopy parameters are not reported in the literature under controlled hydrodynamic conditions and kinetic and thermodynamic parameters under these conditions necessary to compare catalysts were not calculated.

In this work, the results of RDE and electrochemical impedance spectroscopy (EIS) analysis for a polycrystalline nickel catalyst, before and after being subjected to hydrogen evolution conditions for 4 hours in alkaline solution, are reported. Koutecky-Levich, Tafel, and Conway analysis of the RDE results, along with the EIS analysis at different temperatures are discussed with the aim to show how the kinetics and thermodynamic parameters of HER are modified when the nickel catalyst is electrochemically aged under controlled conditions. The theoretical Levich slope was calculated on the basis of the HER mechanism in alkaline solution and used to establish changes in the reaction mechanism with temperature and aging. Calculated kinetic and thermodynamic values are necessary to establish catalysts comparison parameters that help to understand the reason for the improvement or decay of electrocatalytic activity of a catalyst (including alloys) in HER.

2. Experimental

2.1. Chemicals

Potassium hydroxide (Anedra RA reagent), hydrochloric acid 36.5–37% (Cicarelli, PA grade), ethanol 96% (Cicarrelli) were used as received. All aqueous solutions were prepared with Milli-Q water, and degassed using high purity N_2 (Indura S.A.).

2.2. Catalyst preparation

The nickel electrodes (99.9 purity, RC S.A.) for tests (area: 0.196 cm^2) were mechanically polished with alumina powder (0.05 μm). The electrodes were then cleaned repeatedly with ethanol and immersed first in 1 M KOH aqueous solution, and then in HCl (10% w/w) aqueous solution, during 1 minute, in order to degrease the surface prior to use. The area used for all current densities calculation was the corresponding to the geometric area of the disk electrode.

2.3. Structural characterization

Scanning electron micrographs were obtained using a Supra 40 (Zeiss Company) FESEM operating at 3–6 kV, equipped with EDX. EDX spectrum was obtained operating at 6–15 kV.

X-ray diffractograms were measured using the Cu Kα radiation (λ = 1.5406 Å), in a PANalytical X'Pert PRO diffractometer (40 kV, 40 mA), in the θ–2θ Bragg–Brentano geometry at room temperature. The 2θ range was from 10° up to 70°, with increments of 0.02° and a counting time of 1 s per step. The FULLPROF program [28] was applied to refine the crystal structure by the Rietveld method. A pseudo-Voigt shape function was used to fit the experimental data. The data refined were atomic positions, lattice parameters, peak shape, isotropic thermal parameters, and occupation factors.

2.4. Electrochemical characterization

Experiments were carried out in a conventional single compartment three-electrode electrochemical cell. A platinum foil was used as counter electrode and a saturated calomel electrode (SCE) as reference electrode (0.243 V *vs.* RHE). The reference electrode was included in a capillary with gel outside the cell and kept at room temperature. 1 M KOH aqueous solution was used as electrolyte. Electrochemical studies were performed with an Autolab potentiostat/galvanostat model PGStat30 with FRA2 module, coupled to a rotating disk electrode (Pine Research Inst.; Raleigh, NC). The uncompensated ohmic electrolyte resistance (~50 Ω) was measured via high frequency ac impedance in N_2 saturated 1 M KOH, and used to calculate a cell constant. Ohmic drop correction to the applied potentials was perfomed automatically by Autolab software (Metrohm Autolab Nova 1.10). Cell temperature was controlled by a Lauda Alpha RA 8, at several temperatures between 278 K and 303 K.

RDE measurements were conducted on a Ni disk electrode mounted in an interchangeable RDE holder (Pine Instruments).

The rotation rate of the working electrode was varied between 100 and 2500 rpm.

Cyclic voltammetry (CV) and linear sweep voltammetry (LSV) experiments were conducted between 0.1 and −1.5 V (*vs.* SCE) for fresh polished nickel (Ni_f), and between 0.1 and −1.7 V (*vs.* SCE) for nickel post-chronoamperometry (Ni_{pc}), at a scan rate of 10 mV s^{-1}. During the HER measurements a nitrogen flux was maintained above the electrolyte surface.

EIS experiments were conducted by applying a bias of 10 mV at frequencies between 10 mHz and 100 kHz at different electrode potentials such as, open circuit potential (OCP), HER onset potential (OP), and 0.1 V and 0.3 V more cathodic than the corresponding OP of each catalyst. Chronoamperometric measurements were carried out applying −1.5 V (*vs.* SCE) during 4 hours at 298 K. EIS and chronoamperometric experiments were carried out by rotating the electrode at 900 rpm to prevent the formation of bubbles that could generates electrochemical noise.

2.5. Electrochemical analysis

The overall current density, j, of the HER can be expressed in terms of the kinetic current density, j_k, and the boundary-layer diffusion limited current density, j_d. Thus, the overall measured current density can be represented by the Koutecky–Levich (K–L) equation [29]:

$$\frac{1}{j} = \frac{1}{j_k} + \frac{1}{j_d} = \frac{1}{j_k} + \frac{1}{B\omega^{1/2}} \quad (1)$$

where ω is the rotation rate and B is the Levich slope, given by,

$$B = 0.2nFC_o D_o^{2/3} \nu^{-1/6} \quad (2)$$

where ω is expressed in rpm, n is the number of electrons transferred per molecule of H_2O reduced, F the Faraday constant, C_o is the HO^- concentration (0.001 mol cm^{-3}), D_o is the diffusion coefficient of the HO^- ions in the solution (5.3×10^{-5} cm^2 s^{-1}) [30], and ν the kinematic solution viscosity (9.473×10^{-3} cm^2 s^{-1}) [30].

From the slope of the straight lines in the K–L plots, we can evaluate the number of electrons involved in the HER. The theoretical value of the reciprocal Levich slope for a single electron charge transfer ($n = 1$) process to Ni–H_{ad} formation is 1.689×10^{-2} mA^{-1} cm^2 $rpm^{1/2}$.

In order to calculate the j_k, the measured currents were corrected using Eq. (3):

$$j_k = j\left(\frac{j_d}{j_d - j}\right) \tag{3}$$

where $j_d/(j_d - j)$ is the mass transfer correction. The Tafel slope parameter, b, is given by the following equation:

$$b = \frac{2.303RT}{nF\alpha} \tag{4}$$

where n and α are the number of electrons transferred and the transfer coefficient, respectively. It is well known that, the transfer coefficient α varies linearly with temperature,

$$\alpha = \alpha_H + \alpha_S T \tag{5}$$

where α_H is the enthalpic and α_S the entropic component of α. The term α_H is related to the change of electrochemical enthalpy of activation with the electrode potential, meanwhile α_S is related to the change of electrochemical entropy of activation with the potential [31,32]. In order to obtain the α_H and α_s values we resorted to the Conway plot, which is the reciprocal of the Tafel slope *vs.* $1/T$:

$$\frac{1}{b} = \frac{n\alpha_H F}{2.303RT} + \frac{n\alpha_S F}{2.303R} \tag{6}$$

The values of j_0 calculated from the Tafel equation allows to calculate the apparent activation energy ($\Delta H^{\#}$), using the Arrhenius equation represented by the relationship:

$$\Delta H^{\#} = -R\left[\frac{d\ln j_o}{j(1/T)}\right] \tag{7}$$

3. Results and discussion

3.1. Structural characterization

Scanning electron micrographs were obtained to analyze the presence of homogeneous granular structure, or exhibits crevices. Fig. 1a shows the morphology of a fresh polished nickel electrode at a magnification of 100.000 x. The sample is mainly granular and shows polishing marks. No superficial crevices were observed. Energy dispersive X ray spectrum (EDS) (Fig. 1b) shows no metallic contamination and only traces of Al and Si (from the polishing alumina) were found. EDX mapping shows that the composition is homogeneous in the entire sample surface.

The X-ray diffraction pattern (Fig. 1c) for Ni_f clearly shows the characteristic reflections expected for nickel with face centered cubic (fcc) structure [23] without peaks correspondent to impurities. This also reveals that the resultant nanocrystals were

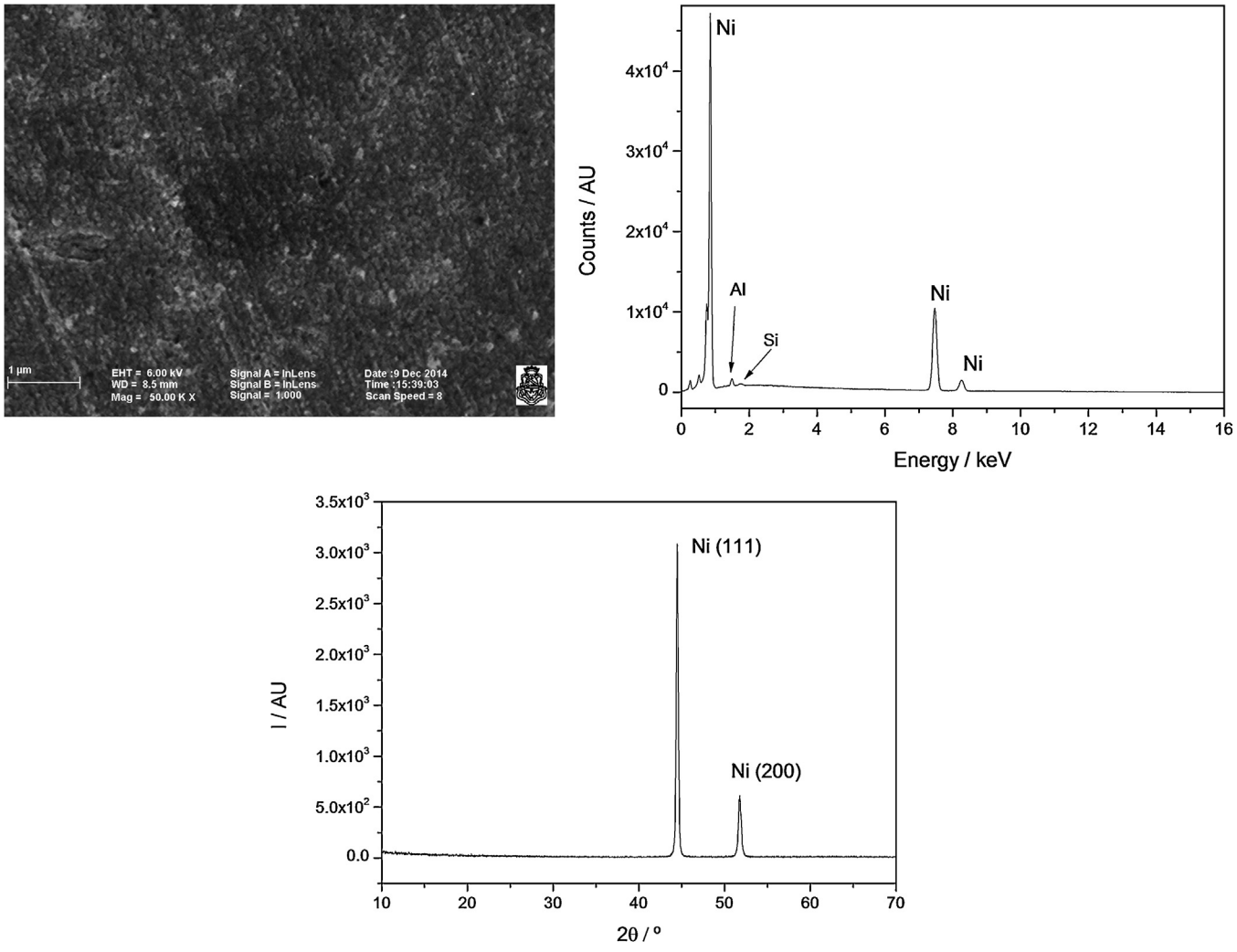

Fig. 1. a SEM micrograph of fresh polished nickel measured at 6 k eV and a magnification of 50.000 x b: EDS spectrum of Ni_f measured at 15 k eV c: X-ray diffraction pattern of Ni_f.

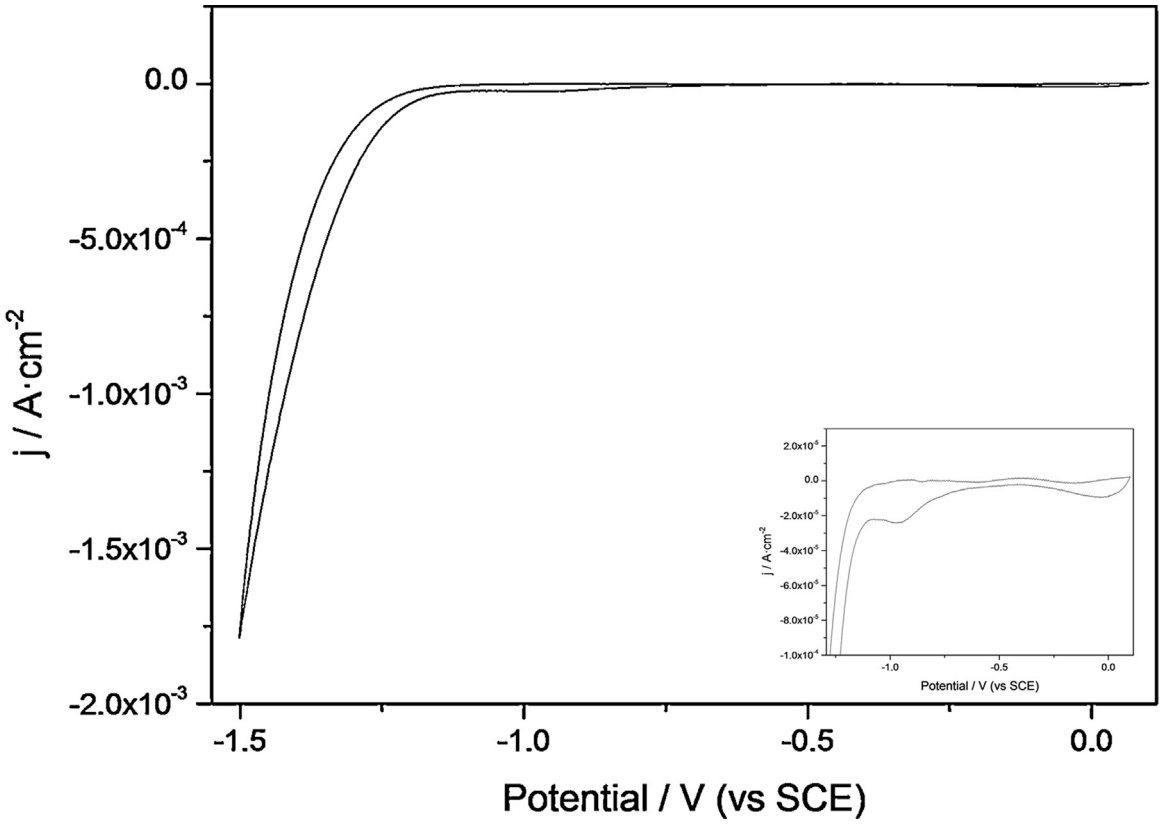

Fig. 2. Cyclic voltammogram of Ni_f catalyst in 1 M KOH at 298 K (scan rate: 10 mV s^{-1}). Insert: Magnification of the cyclic voltammogram.

that of pure fcc nickel. The ratio of intensities of the XRD peaks of 1 1 1 and 2 0 0 planes is 5.61 showing a preferential 1 1 1 plane in the fresh polished catalyst. The respective values of 2θ, for the planes 1 1 1 and 2 0 0 are 44.5° (FWHM = 0.2165°) and 51.8° (FWHM = 0.0984°), respectively; with a d-spacing distance of 2.04 Å for the plane 1 1 1 and 1.76 for the 2 0 0 plane.

3.2. Cyclic voltammetric and chronoamperometric analysis

Fig. 2 shows a typical cyclic voltammogram obtained for Ni_f in 1 M KOH solution, where the onset potential for the hydrogen evolution, *c.a.* −1.1 V (*vs.* SCE) is in good agreement with the known value for nickel [33,34]. A zoom of the CV is shown in the insert on Fig. 2, where a peak can be observed at approximately −0.9 V (vs. SCE) in the cathodic sweep, which is associated with H atoms adsorption on the nickel surface[35].

This electrode, after being characterized for different electrochemical techniques (LSV by RDE at different temperatures, EIS at different potentials), was subjected to a potential pulse, in order to analyze short-term aging effect of the catalyst during the hydrogen evolution. In Fig. 3, the hydrogen generation chronoamperometry of the Ni catalyst is shown, and two zones can be clearly individualized. The first one, between 0 and 100 s, where the current decreases rapidly, and the second one, for t > 100 s, where a gradual increase of the hydrogen generation current is observed, respectively.

Fig. 4 shows the comparison of LSV for Ni_f and Ni_{pc} electrodes. Following the chronoamperometry pulse, a −0.3 V shift of the HER

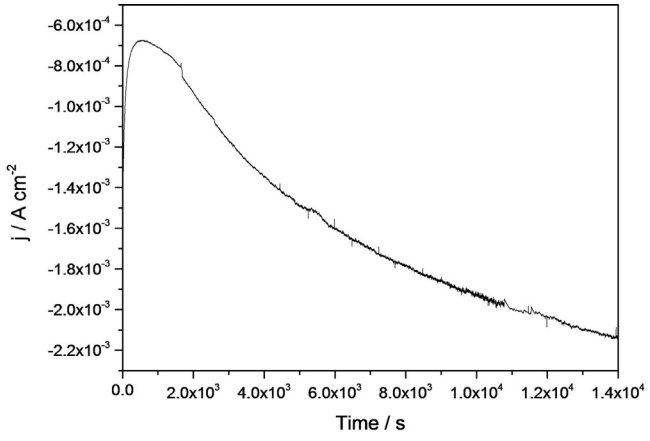

Fig. 3. Chronoamperometric profile of hydrogen evolution reaction on Ni_f in 1 M KOH obtained at −1.5 V (*vs.* SCE), 298 K, and rotation speed of 900 rpm.

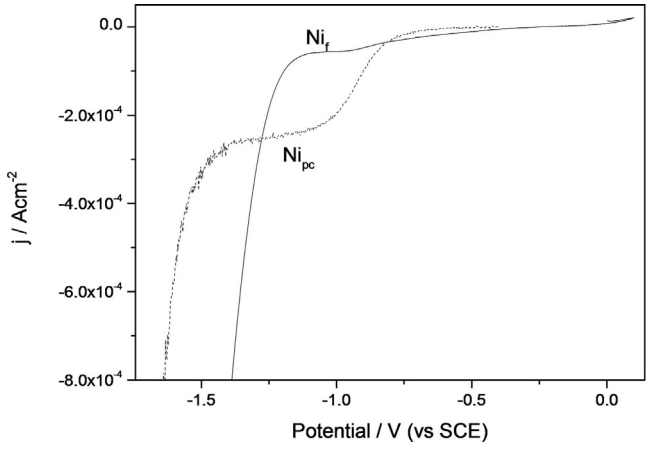

Fig. 4. LSV of Ni_f (filled line) and Ni_{pc} (dashed line) electrodes in 1 M KOH measured at 298 K (scan rate: 10 mV s^{-1}).

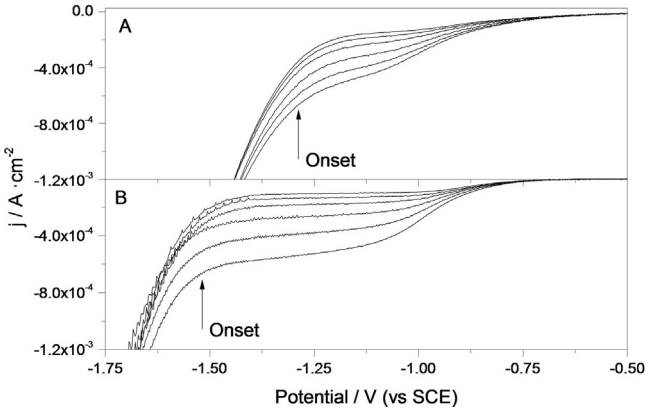

Fig. 5. Current potential curves for HER obtained in 1 M KOH at 298 K on: a) Ni_f; b) Ni_{pc}, at different rotation rates.

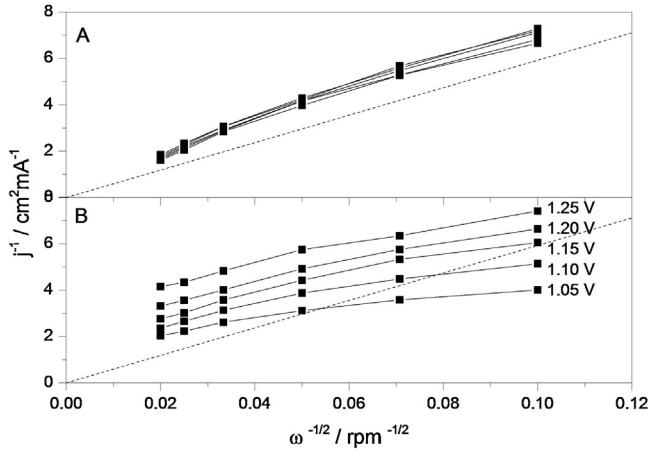

Fig. 6. K-L plots for HER at 298 K on a) Ni_f and b) Ni_{pc} at different electrode potentials. In dashed line, the theoretical one electron slope is showed.

onset potential (−1.4 V *vs.* SCE), is observed in comparison with Ni_f. Additionally, the hydrogen adsorption onset maintains its potential value (−0.9 V), but the H_2O adsorption current considerably increases its intensity (from −0.9 to −1.45 V (vs. SCE)). These results shows that, under the present conditions, the H adsorption reaction (Volmer reaction) is activated, as indicated by the increase in the chronoamperometric current, while the H_2 release reaction is hindered.

3.3. RDE analysis

Fig. 5 shows a set of RDE current density-potential curves obtained on Ni_f and Ni_{pc} catalysts in N_2-saturated 1 M KOH at 298 K. Both catalysts show a well-defined charge-transfer kinetic control at potentials above -0.77 (*vs.* SCE) and a mixed kinetic diffusion control occurring in the range of -1.03 to -0.77 V (*vs.* SCE). Significant differences between the electrochemical behavior of Ni_f and Ni_{pc} catalysts are observed at more cathodic potential, where the mass transport-limited currents became noticeable and a dependence of the current density with the rotation rate is observed. In the case of Ni_f catalyst, the limiting currents are not well defined, indicating that different processes could be occurring in the catalyst surface, in addition to those associated with the H_2 generation, such as the incorporation of hydrogen into the surface (hidruration), adsorption of species, poisoning by impurities, etc. [36]. On the other hand, much better defined limiting currents are observed for the Ni_{pc} catalyst. The curves show a shifting in the onset potential of hydrogen evolution. As the rotation rate increased, limiting currents also increased, as a result of a faster diffusion to the electrode surface.

In Table 1, the experimental values of Levich slope for Ni_f and Ni_{pc} from Fig. 6 are shown, along with the calculated values of n at each temperature. Besides, it can be seen that for Ni_f $n \approx 1$ at almost all temperatures, while for the Ni_{pc} catalyst n exhibits a marked dependence with the temperature, which is consistent with a mechanism where the water adsorption on the catalyst surface is the limiting step [37].

Fig. 7a shows the Tafel plots corrected by the mass transport for Ni_f and Ni_{pc} catalysts, obtained from the measured current in the mixed activation–diffusion region.

Table 1
Kinetics parameters (*) for the HER on Ni_f and Ni_{pc} catalysts in 1 M KOH calculated from the K-L analysis and Tafel slope (* average values from all rotation rates).

	Ni_f				Ni_{pc}			
T	B	n	Tafel/V dec^{-1}	α	B	n	Tafel/V dec^{-1}	α
278	0.0147	0.86	−0.214	0.30	0.01689	1	−0.122	0.45
283	0.01689	1	−0.234	0.24	0.01485	0.9	−0.133	0.47
288	0.01688	0.99	−0.241	0.24	0.01293	0.79	−0.134	0.54
293	0.01689	1	−0.249	0.23	0.01148	0.71	−0.138	0.59
298	0.01689	1	−0.281	0.21	0.01049	0.64	−0.167	0.55
303	0.01639	0.97	−0.318	0.19	0.01098	0.68	−0.162	0.54

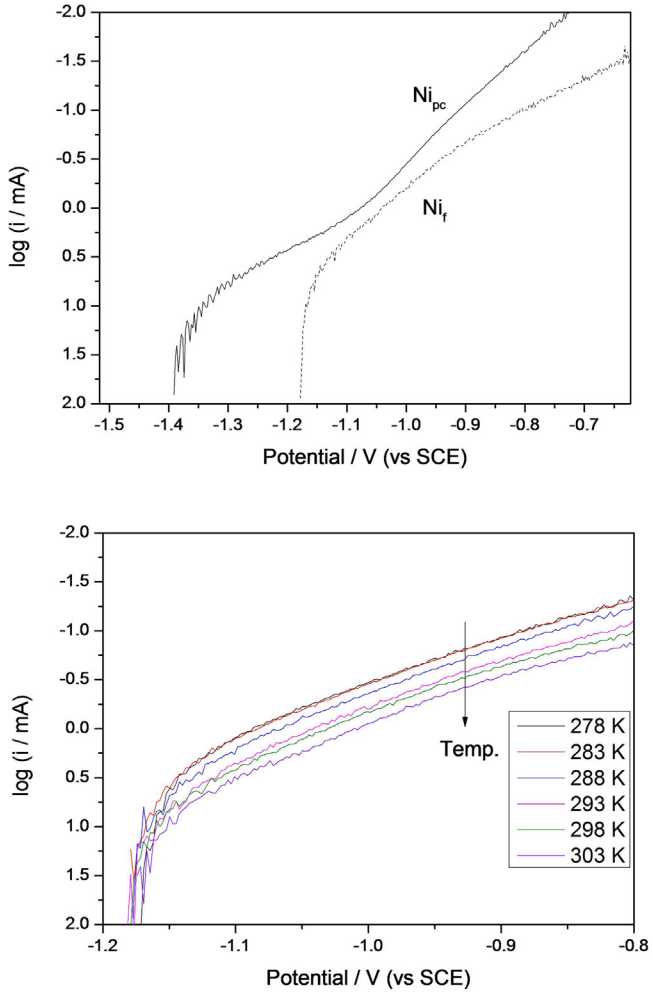

Fig. 7. a Tafel plots corrected by mass transfer for the HER on Ni_f (filled line) and Ni_{pc} (dashed line) at 1600 rpm and 293 K. b: Tafel plots corrected by mass transfer for the HER on Ni_f at 1600 rpm as a function of the temperature. Scan rate = 10 mV s^{-1}.

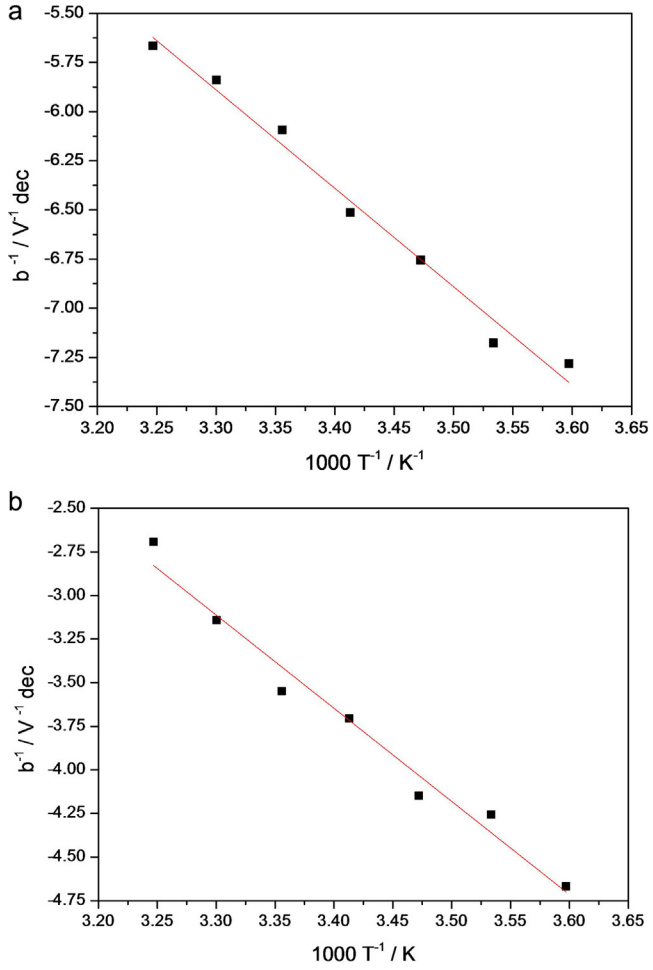

Fig. 8. Conway plots of the reciprocal Tafel slope (b) *vs.* T^{-1} for the Ni_f (Fig. 8a) and Ni_{pc} catalysts (Fig. 8b). The values of *b* were taken from Fig. 6.

Kinetic parameters such as the Tafel slope, transfer coefficient, exchange current density and activation energy were evaluated as a function of temperature [32,38], and the corresponding results are summarized in Table 1. The Tafel slopes presented were obtained as the average of the Tafel slopes at all the rotation rates.

Fig. 7b shows the mass transfer corrected Tafel plots at several temperatures and 1600 rpm for the Ni_f catalyst in 1 M KOH solution. The increase of current densities with temperature reflects temperature-activated chemical rate constant. The Tafel slope at each temperature shows a linear behavior at high current densities, and the kinetic parameters were determined from these data, yielding mean Tafel slopes of $-0.256\,V\,dec^{-1}$ for Ni_f and $-0.142\,V\,dec^{-1}$ for Ni_{pc}. The Tafel slopes increases monotonically with the temperature, probably because the structure of the catalyst is being modified, besides the processes related to HER occurring on the electrode surface.

The variation of the transfer coefficient with respect to the absolute temperature (T^{-1}) determined from data in Table 1 is $d\alpha/dT = 3.53 \times 10^{-3}\,K^{-1}$ and $5.86 \times 10^{-3}\,K^{-1}$ for Ni_f and Ni_{pc}, respectively.

Table 2
Thermodynamic parameters of the transference coefficients calculated from the Conway plots.

	α_H	α_S/K^{-1}
Ni_f	-1.13×10^{-3}	3.11×10^{-3}
Ni_{pc}	-9.92×10^{-4}	2.11×10^{-3}

Table 3
Exchange currents density calculated for both catalysts at different temperatures.

	j_0/mA cm^{-2} (at 100 rpm)	
T (K)	Ni_f	Ni_{pc}
278	5.47×10^{-6}	6.33×10^{-9}
283	1.82×10^{-5}	2.32×10^{-8}
288	2.19×10^{-5}	2.74×10^{-8}
293	3.69×10^{-5}	3.87×10^{-8}
298	1.21×10^{-4}	6.91×10^{-7}
303	2.78×10^{-4}	2.74×10^{-7}

Fig. 8 shows the Conway plots corresponding to Ni_f and Ni_{pc}. In Table 2, the α_H and α_S parameters obtained for both, Ni_f and Ni_{pc} from the corresponding Conway plots are summarized. For both electrocatalysts the results suggest a predominant contribution of the entropic part in this electrochemical process, probably through the double layer structure, as described by Conway [39]. The negative α_H values indicate a positive heat of adsorption, while $\alpha_s > 0$ suggests an increase in the disorder of the system during the activation, due to the Tafel reaction, since that reaction generates H_2 and consumes H_{ad} atoms generated during the Volmer reaction, responsible for ordering system.

Table 3 shows the results of the exchange current density (j_0) obtained from the Tafel analysis. It can be seen that the exchange current density for Ni_f is three orders of magnitude greater than that found for Ni_{pc}, which indicates a deactivation of the catalyst activity after a chronoamperometric pulse.

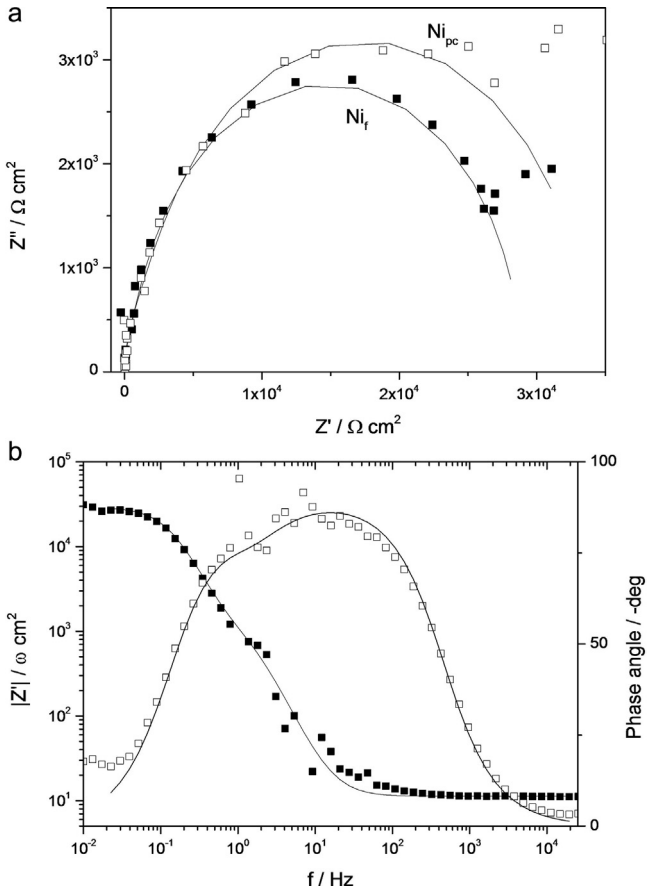

Fig. 9. a Impedance spectra in the complex plane for the HER on Ni_f (filled dots) and Ni_{pc} (open dots) in 1 M KOH at 298 K and at a rotation rate of 900 rpm, at the OCP (correspondent at each catalyst). b: Bode plot for the Ni_f catalyst in 1 M KOH at 298 K and at a rotation rate of 900 rpm and at the OCP. The filled square corresponds to Z' and the open squares corresponds to the measured phase angle. The solid lines are calculated using the AHEC.

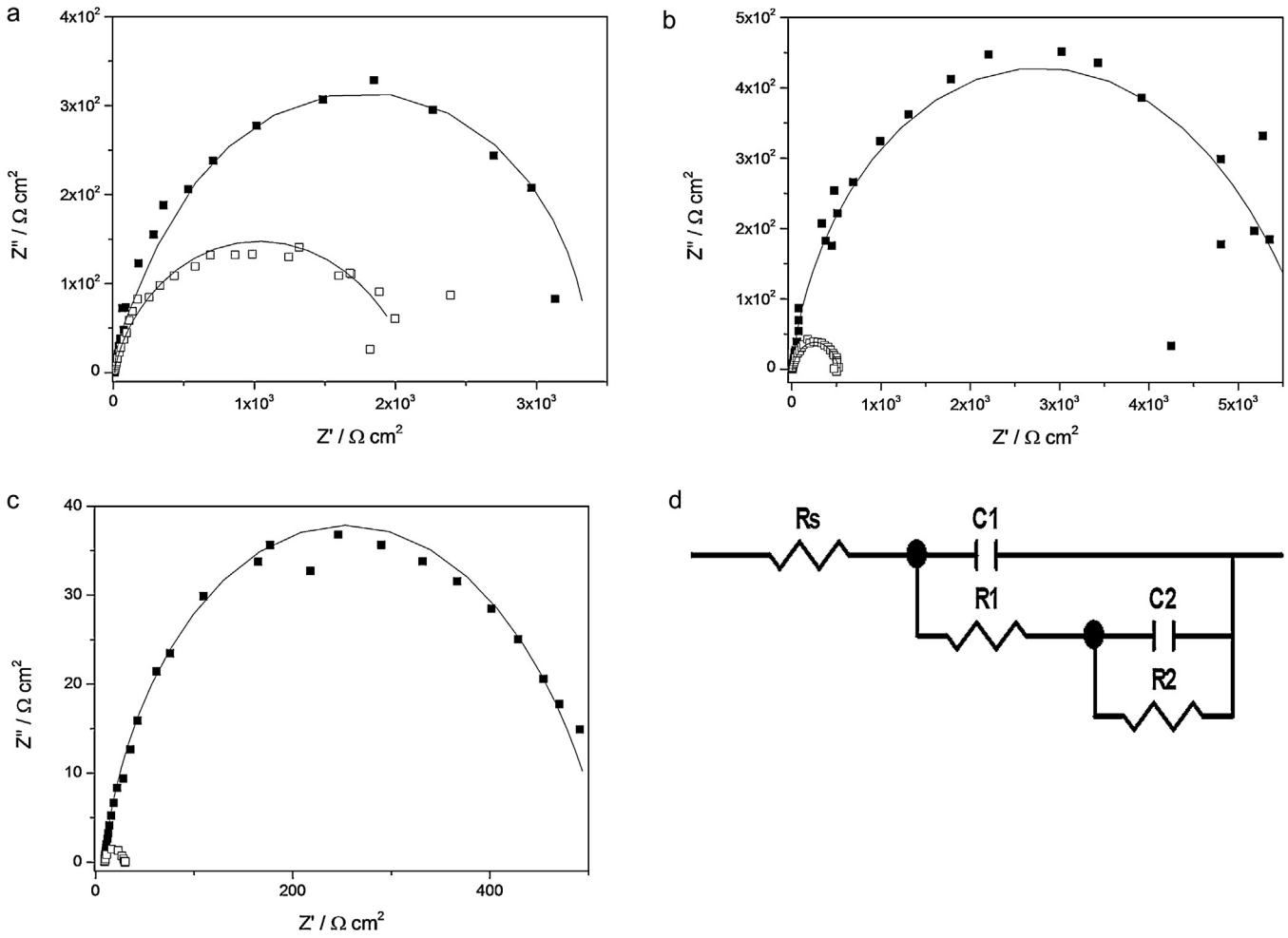

Fig. 10. Impedance spectra in the complex plane for the HER on Ni_f (filled dots) and Ni_{pc} (open dots) in 1 M KOH at 298 K and at a rotation rate of 900 rpm, at different potentials. a) Onset potential of HER. b) overpotential 0.1 V higher that the corresponding onset potential. c) overpotential 0.3 V higher that the corresponding onset potential. d) Armstrong and Henderson equivalent electric circuit.

The apparent activation energy, $\Delta H^{\#}$ (Eq. (7)), for the HER on Ni_f and Ni_{pc} electrocatalysts was evaluated from the slope of the Arrhenius plot (data from Table 3). Average apparent activation energies of $60.3 \pm 0.5\,kJ\,mol^{-1}$, and $65.3 \pm 0.5\,kJ\,mol^{-1}$ were calculated for Ni_f and Ni_{pc}, respectively. It can be seen that the activation energy obtained for the HER on Ni_f is lower than that obtained on Ni_{pc}, which is consistent with the decrease in current observed in Ni_{pc}.

3.4. EIS analysis

The electrochemical impedance spectrum in the complex plane recorded at open circuit potential ($E = -0.25$ V), for Ni_f and Ni_{pc} are consistent with a charge transfer controlled process (Fig. 9a) [35].

Table 4
Parameters of the AHEC for the HER at Ni_f and Ni_{pc} in 1 M KOH at 298 K.

Catalyst	E/V (SCE)	$R_1/\Omega\,cm^2$	$R_2/\Omega\,cm^2$	$C_p/\mu F\,cm^{-2}$	$C_{dl}/\mu F\,cm^{-2}$
Ni_f	−0.25 (OCP)	9473.1	19374.0	30.8	19.2
	−1.1 (Onset)	1117.2	2248.7	103.4	106.7
	−1.2	185.1	4752.8	114.6	31.3
	−1.4	100.9	320.7	232.0	214.7
Ni_{pc}	−0.24 (OCP)	11712.2	22030.4	33.2	30.1
	−1.35 (Onset)	685.4	1163.7	238.2	637.3
	−1.45	205.4	270.7	323.9	678.5
	−1.65	10.4	7.7	562.3	1620.0

Fig. 9b shows the Bode diagram corresponding to the spectrum at the onset potential for Ni_f and the fit obtained using the Armstrong and Henderson equivalent circuit (AHEC) [40].

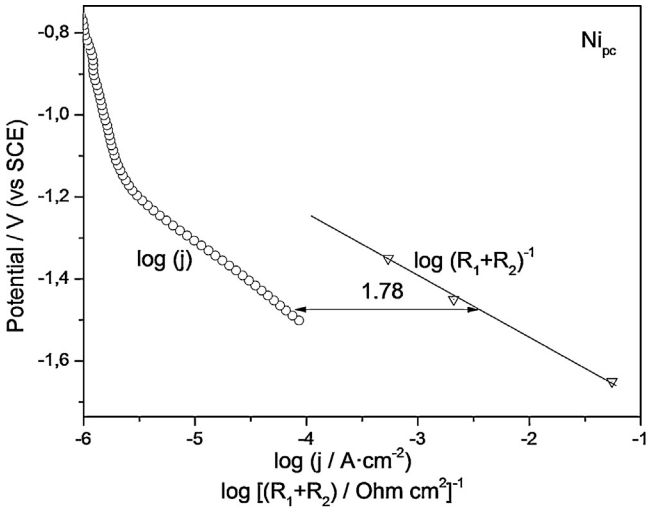

Fig. 11. Experimental Tafel plot (circled points) and simulated E-$\log(R_1 + R_2)^{-1}$ plot (triangles) with the corresponding linear fir (solid line) for the HER on Ni_{pc} in 1 M KOH solution at 298 K.

The impedance spectra in the complex plane were also determined at three values of electrode potentials, selected to cover the entire reaction region: the onset potential of the HER (for each catalyst), and potentials 0.1 V and 0.3 V more cathodic than the corresponding onset. Fig. 10a, b, and c show the impedance spectra in the complex plane for the selected potentials in the HER region. Fig. 10d shows the AHEC, where R_s is the solution resistance, R_1 is the charge transfer resistance for the electrode reaction, C_1 the double layer capacitance, R_2 is related to the superficial mass transfer resistance of the H_{ad}, and C_2 is the pseudo-capacitance. In the AHEC, the Faradaic impedance, Z_f is defined as:

$$Z_f = R_1 + \frac{R_2}{1 + j\omega\tau_p} \quad (8)$$

where ω is the frequency and $\tau_p = R_2C_2$ is the time constant related to the relaxation rate when the potential is changed. The parameters obtained by the fit of results with the AHEC are shown in Table 4. There is a noticeable change in the charge transfer resistance and capacitance after the chronoamperometric pulse; this is due to the enhancement of charge transfer to generate H_{ad} (as seen above). Variations in the capacitance may be associated with a change in the type of H adsorption, related with the surface hidruration.

The sum $R_1 + R_2$ (at the same potential) represents the total Faradaic resistance which is related with the kinetics of HER, and its reciprocal is directly related to the Faradaic current density. Since the HER is charge transfer controlled within the considered potential region, the E *vs.* $\log(R_1 + R_2)^{-1}$ plot should be linear, and its slope equal to the Tafel slope, b. Fig. 11 shows this plot for Ni_{pc}, along with the Tafel plot obtained by cyclic voltammetry (without mass transfer correction). It can be seen that the conventional Tafel plot and the simulated E *vs.* $\log(R_1 + R_2)^{-1}$ plot are almost parallel lines separated at the abscissa. The separation observed for Ni_f was 1.16, while the founded for Ni_{pc} was 1.78.

Conway and coworkers [41] have shown that the theoretical separation for Langmuir type adsorption is equal to $\log(\beta F/RT)$. For $\beta = 0.5$ and $T = 298$ K, $\log(\beta F/RT) = 1.289$, which is close to the experimental value observed for Ni_f. However, the separation of 1.78 founded in Ni_{pc} approaches to a Temkin adsorption isotherm (characterized by a theoretical separation of 1.86) [41].

These experimental evidences would indicate a change in the H adsorption, from a Langmuir monolayer adsorption in the freshly polished electrode, to a Temkin adsorption in Ni_{pc}. The later is characterized by a decrease of the adsorption heat due to interactions between the adsorbates [16]. This behavior could be originated by the modification of the electrode surface forming a hydride, which would stabilize the subsequent adsorption of H. The effect of stabilization is also noted in the fact that the current of H_{ad} generation in Fig. 4 (−0.95 to −1.1 V) increases after chronoamperometry showing a larger amount of H_{ad}. Additionally, the shift of HER onset potential from −1.1 to −1.4 V is consistent with greater stability H_{ad} the hydride on the surface of nickel.

4. Conclusions

In this paper a new approach to the analysis for the mechanism of hydrogen evolution reaction on nickel electrodes in alkaline solutions is presented. The results of EIS and RDE electrochemical characterization of the HER on a freshly polished nickel catalyst and the same catalyst following hydrogen evolution potential during 4 hours, are analyzed.

It was possible to observe large changes in the electrocatalytic behavior of nickel after the chronoamperometry. These changes in the electrochemical response were correlated with changes in the H adsorption rate on the catalyst surface.

The Koutecky Levich analysis allowed to observe modifications in the reaction mechanism with temperature and aging, evidenced by the number of transferred electrons, which have not been determined by other electrochemical techniques. For that purpose we have developed the necessary theory for calculating the theoretical Levich slopes corresponding to the mechanism. It has been shown that the calculated Levich constant for the nickel catalyst in alkaline solution can be applied to nickel catalysts even when they have been aged, and can be used as the benchmark for future work helping elucidate mechanisms HER in other catalysts.

The complementation of the RDE analysis with impedance spectroscopy allows us to analyze changes in the HER mechanism in different catalysts, but also analyze changes the way in which the H is adsorbed on the nickel surface, information which until now had not been fully reported.

The results of the Tafel and Koutecky-Levich analysis show that the rate determining step on Ni_f is one electron transfer process during the Volmer reaction, showing a Langmuir type H adsorption isotherm. On the other hand, on Ni_{pc}, the number of transferred electrons decreases, showing a marked temperature dependence, while the H adsorption isotherm is Temkin type, allowing us to establish how changes in the adsorption type generate changes in the reaction mechanism, in the activation energy and activation parameters α_H and α_S.

Acknowledgements

The authors thank financial support from Agencia Nacional de Promoción Científica y Tecnológica, and CONICET (PIP 00095). H.C., G.L., and E.F. are permanent research fellows of CONICET. The authors thank to LAMARX laboratory for its assistance in SEM/EDX measures, and to Dr. Raul Carbonio and Dra. Cecilia Blanco for XRD measures.

References

[1] Y. Miao, L. Ouyang, S. Zhou, L. Xu, Z. Yang, M. Xiao, R. Ouyang, Electrocatalysis and electroanalysis of nickel, its oxides, hydroxides and oxyhydroxides toward small molecules, Biosens. Bioelectron. 53 (2014) 428–439.
[2] P.M. Quaino, M.R. Gennero de Chialvo, A.C. Chialvo, Hydrogen electrode reaction: A complete kinetic description, Electrochim. Acta 52 (2007) 7396–7403.
[3] Y. Petrov, J.-P. Schosger, Z. Stoynov, F. de Bruijn, Hydrogen evolution on nickel electrode in synthetic tap water–alkaline solution, Int. J. Hydrogen Energ. 36 (2011) 12715–12724.
[4] U.C. Lacnjevac, B.M. Jovic, V.D. Jovic, N.V. Krstajic, Determination of kinetic parameters for the hydrogen evolution reaction on the electrodeposited Ni–MoO_2 composite coating in alkaline solution, J. Electroanal. Chem. 31 (2012) 677–680.
[5] L. Bai, D.A. Harrington, B.E. Conway, Behavior of overpotential – deposited species in Faradaic reactions – II. ac Impedance measurements on H_2 evolution kinetics at activated and unactivated Pt cathodes, Electrochim. Acta 32 (1987) 1713–1731.
[6] D.E. Hall, Porous Nickel-Coated Steel Anodes for Alkaline Water Electrolysis: Corrosion Resistance, J. Electrochem. Soc.: Electrochem. Sci. Technol. 129 (1982) 310–315.
[7] C. Graves, S.D. Ebbesen, M. Mogensen, K.S. Lackner, Sustainable hydrocarbon fuels by recycling CO_2 and H_2O with renewable or nuclear energy, Renew. Sustain. Energy Rev. 15 (2011) 1–23.
[8] G. Gahleitner, Hydrogen from renewable electricity: An international review of power-to-gas pilot plants for stationary applications, Int. J. Hydrogen Energ. 38 (2013) 2039–2061.
[9] B. Losiewicz, A. Budniok, E. Rowinski, E. Lagiewka, A. Lasia, The structure, morphology and electrochemical impedance study of the hydrogen evolution reaction on the modified nickel electrodes, Int. J. Hydrogen Energ. 29 (2004) 145–157.
[10] D.A. Harrington, B.E. Conway, A.C. Impedance of Faradaic Reactions Involving Electrosorbed Intermediates; Part I: Kinetic Theory, Electrochim. Acta 3212 (1987) 1703–1712.
[11] G. Kreysa, B. Hakansson, P. Ekdunge, Kinetic and thermodynamic analysis of hydrogen evolution at nickel electrodes, Electrochim. Acta 33 (1988) 1351–1357.
[12] V. Wendt, H. Plzak, Electrocatalytic and thermal activation of anodic oxygen- and cathodic hydrogen-evolution in alkaline water electrolysis, Electrochim. Acta 28 (1983) 27–34.

[13] A.J. Appleby, M. Chemla, H. Kita, G. Bronoel, Encyclopedia of Electrochemistry of the Elements, in: N.Y. Bard (Ed.), Marcel Dekker, NY, USA, 1982.
[14] J. Jacquelin, A.J. Appleby, Nouvelles perspectives dansl'électrolyse de l'eau, Rev. Generalel'Electricite 85 (1976) 551–554.
[15] G. Kreysa, B. Hakansson, Electrocatalysis by amorphous metals of hydrogen and oxygen evolution in alkaline solution, J. Electroanal. Chem. 201 (1986) 61–83.
[16] U.C. Lacnjevac, B.M. Jovic, V.D. Jovic, V.R. Radmilovic, N.V. Krstajic, Kinetics of the hydrogen evolution reaction on Ni-(Ebonex-supported Ru) composite coatings in alkaline solution, Int. J. Hydrogen Energ. 38 (2013) 10178–10190.
[17] L. Vázquez-Gómez, S. Cattarin, P. Guerriero, M. Musiani, Influence of deposition current density on the composition and properties of electrodeposited $Ni+RuO_2$ and $Ni+IrO_2$ composites, J. Electroanal. Chem. 634 (2009) 42–48.
[18] L. Vázquez-Gómez, S. Cattarin, P. Guerriero, M. Musiani, Hydrogen evolution on porous Ni cathodes modified by spontaneous deposition of Ru or Ir, Electrochim. Acta 53 (2008) 8310–8318.
[19] M.A. Dominguez-Crespo, E. Ramírez-Meneses, A.M. Torres-Huerta, V. Garibay-Febles, K. Philippot, Kinetics of hydrogen evolution reaction on stabilized Ni, Pt and Ni-Pt nanoparticles obtained by an organometallic approach, Int. J. Hydrogen Energ. 37 (2012) 4798–4811.
[20] R.M. Abouatallah, D.W. Kirk, S.J. Thorpe, J.W. Graydon, Reactivation of nickel cathodes by dissolved vanadium species during hydrogen evolution in alkaline media, Electrochim. Acta 47 (2001) 613–621.
[21] S.A.S. Machado, J. Tiengo, P. de Lima Neto, L.A. Avaca, The influence of H-absorption on the cathodic response of high area nickel electrodes in alkaline solutions, Electrochim. Acta 39 (1994) 1757–1761.
[22] H.E.G. Rommal, P.J. Morgan, The role of absorbed hydrogen on the voltage-time behavior of nickel cathodes in hydrogen evolution, J. Electrochem. Soc. 135 (1988) 343–346.
[23] H.E.G. Rommal, P.J. Moran, Time-dependent energy efficiency losses at nickel cathodes in alkaline water electrolysis systems, J. Electrochem.Soc. 132 (1985) 325–329.
[24] D.M. Soares, O. Teschke, I. Torriani, Hydride effect on the kinetics of the hydrogen evolution reaction on nickel cathodes in alkaline media, J. Electrochem. Soc. 139 (1992) 98–105.
[25] A.C. Makrides, Hydrogen overpotential on nickel in alkaline solution, J. Electrochem. Soc. 109 (1962) 977–984.
[26] S.A.S. Machado, L.A. Avaca, The hydrogen evolution reaction on nickel surfaces stabilized by H-absorption, Electrochim. Acta 39 (1994) 1385–1391.
[27] D.S. Hall, C. Bock, B.R. MacDougall, The electrochemistry of metallic nickel: oxides, hydroxides, hydrides and alkaline hydrogen evolution, J. Electrochem. Soc. 160 (2013) F235–F243.
[28] J. Rodríguez-Carvajal, Recent Advances in Magnetic Structure Determination by Neutron Powder Diffraction, Physica B 192 (1993) 55–69.
[29] E.A. Franceschini, M.M. Bruno, F.A. Viva, F.J. Williams, M. Jobbágy, H.R. Corti, Mesoporous Pt electrocatalyst for methanol tolerant cathodes of DMFC, Electrochim. Acta 71 (2012) 173–180.
[30] W.M. Haynes, CRC Handbook of Chemistry and Physics, 94th Edition, CRC Press, 2013.
[31] A. Damjanovic, Temperature dependence of symmetry factors and the significance of experimental activation energies, J. Electroanal. Chem. 355 (1993) 57–77.
[32] K. Suarez-Alcantara, O. Solorza-Feria, Kinetics and PEMFC performance of RuxMoySez nanoparticles as a cathode catalyst, Electrochim. Acta 53 (2008) 4981–4989.
[33] I. Bianchi, E. Guerrini, S. Trasatti, Electrocatalytic activation of Ni for H2 evolution by spontaneous deposition of Ru, Chemical Physics 319 (2005) 192–199.
[34] A. ðukic, V. Alar, M. Firak, S. Jakovljevic, A significant improvement in material of foam, J. Alloy. Compd. 573 (2013) 128–132.
[35] N. Krstajic, M. Popovic, B. Grgur, M. Vojnovic, D. Sepa, On the kinetics of the hydrogen evolution reaction on nickel in alkaline solution - part I. the mechanism, J. Electroanal. Chem. 512 (2001) 16–26.
[36] P. Sotelo-Mazón, R.G. González-Huerta, J.G. Cabañas-Moreno, O. Solorza-Feria, Mechanically milled RuxFey Electrocatalyst for Oxygen Reduction in acid media, Int. J. Electrochem. Sci. 2 (2007) 523–533.
[37] N. Krstajic, M. Popovic, B. Grgur, M. Vojnovic, D. Sepa, On the kinetics of the hydrogen evolution reaction on nickel in alkaline solution - part II. effect of temperature, J. Electroanal. Chem. 512 (2001) 27–35.
[38] K. Suarez-Alcantara, O. Solorza-Feria, Evaluation of $Ru_xW_ySe_z$ Catalyst as a Cathode Electrode in a Polymer Electrolyte Membrane Fuel Cell, Fuel Cells 10 (2010) 84–92.
[39] B.E. Conway, D.F. Tessier, D.P. Wilkinson, Temperature dependence of the Tafel slope and electrochemical barrier symmetry factor beta, in electrode kinetics, J. Electroanal. Chem. 136 (1989) 2486–2492.
[40] R.D. Armstrong, M. Henderson, Impedance plane display of a reaction with an adsorbed intermediate, J. Electroanal. Chem. 39 (1972) 81–90.
[41] L. Bai, D.A. Harrington, B.E. Conway, Behaviour of Overpotential-Deposited Species in Faradaic Reactions - Part II.A.C. Impedance Measurements on H_2 Evolution Kinetics at Activated and Unactivated Pt Cathodes, Electrochim. Acta 32 (1987) 1713–1731.